suspension was filtered through Sartorius SM 11607 regenerated cellulose membrane filters (0.45-μm mean pore size) and the residue washed once with H_2O (15 mL) and twice with acetone (2 × 15 mL). The total preparation time was typically 50 min. Anal. Calcd for $Cr_3(\mu\text{-}OH)_4(OH)_5(OH_2)_4\cdot 4H_2O$: Cr, 34.42; ClO_4^-, 0. Found: Cr, 33.69 (±0.03); ClO_4^-, 2.0 (±0.1). Washing of the sample prior to analysis reduced the ClO_4^- content to 1.2%, a value closer to that found for the "active" dimer hydroxide.[11] As for the "active" dimer hydroxide,[11] the purity of "active" trimer hydroxide samples was determined by using ion-exchange chromatography.

A number of experiments were designed to study how the solid-state aging of the "active" trimer hydroxide might be affected by drying. Dehydration of the "active" trimer hydroxide was followed by measuring losses in weight of a sample (ca. 100 mg) after progressively longer dessication periods over 11 M H_2SO_4 (Table I). From time to time samples of the "active" hydroxide were analyzed, with use of using established methods,[11] to determine any changes in composition that accompanied the dehydration process (Table II).

Aging Experiments. Suspensions of the "active" trimer hydroxide were prepared by adding rapidly, with stirring, the hydrolytic trimer (5 mL, $[Cr(III)]_T = 0.0328$ M, $[H^+] = 0.032$ M, and $[Na^+] = 1.85$ M) to 5 mL of each buffer solution. The final pH values of these suspensions were in the range 5.50-11.76. A different procedure was followed for aging experiments at pH 5.15; viz., 10 mL of trimer was diluted to 20 mL (I = 1.0 M) and then brought to the correct pH by adding 0.1 M NaOH (0.9 M $NaClO_4$ added to maintain I = 1.0 M). During the aging period a pH stat was used to maintain constant pH. In all cases, suspensions were aged for periods of 1, 5, or 30 min at 25.0 (±0.1) °C, followed by quenching with 5 M $HClO_4$ (1-2 mL) and analysis by ion-exchange chromatography.[9,10] Three distinct fractions were eluted: trimer (2 M $NaClO_4$, 0.02 M H^+), hexamer (4 M $LiClO_4$, 0.04 M H^+), and higher oligomers (saturated $K_2C_2O_4$ and 0.2 M NaOH). The Cr content of each band was determined as before.[9]

Acknowledgment. This work was supported by the Swiss National Science Foundation (Grant 2.838-0.83). We wish to express our gratitude to A. L. Toko and Drs. H. Stünzi and F. P. Rotzinger for preliminary measurements on chromite cleavage and Dr. G. D. Campbell for valuable comments.

Registry No. 1, 78939-63-6; $[Cr(OH_2)_6](ClO_4)_3$, 27535-70-2; $Cr_3(\mu\text{-}OH)_4(OH)_5(OH_2)_4\cdot 4H_2O$, 114978-36-8.

Supplementary Material Available: The distribution of oligomeric products generated by acid cleavage of chromite solutions (Table S1) and the pH and time dependence of the oligomers formed on aging of the "active" trimer hydroxide (Table S2) (3 pages). Ordering information is given on any current masthead page.

Contribution from the Department of Chemistry, Northwestern University, Evanston, Illinois 60208

Characteristic Vibrational Frequencies and Normal Modes of the CCO Ligand in Trinuclear Ketenylidene Clusters

Michael J. Sailor, Michael J. Went, and Duward F. Shriver*

Received February 26, 1988

The two stretching vibrations associated with the CCO ligand in $[PPN]_2[Ru_3(CO)_6(\mu\text{-}CO)_3(\mu_3\text{-}CCO)]$ (**1**) have been identified by isotopic substitution and fit to an approximate normal-coordinate analysis. The high-frequency CCO stretching component occurs in the carbonyl stretching region (1977 cm^{-1}), and significant mixing occurs between this CCO stretch and a terminal carbonyl stretch of the same symmetry. The low-frequency CCO stretching vibration has been identified in the Raman spectrum of **1** and in the IR or Raman spectra of the ketenylidene clusters $H_2Ru_3(CO)_9(\mu_3\text{-}CCO)$, $[PPN]_2[Fe_3(CO)_9(\mu_3\text{-}CCO)]$, and $[Co_3(CO)_9(\mu_3\text{-}CCO)][PF_6]$. This mode was found in the 1200-1350-cm^{-1} range, with the more positively charged clusters having lower frequencies. The position of the high-frequency CCO stretch of $[PPN]_2[Ru_3(CO)_6(\mu\text{-}CO)_3(\mu_3\text{-}CCO)]$ is sensitive to isotopic substitution at the central carbon atom of the CCO but relatively unaffected by ^{13}C substitution at the basal carbon. The converse is true for the low-frequency CCO stretch. This pattern of isotope shifts has a simple explanation in the form of the normal modes, and it should prove useful in the search for CCO on metal surfaces. Several of the framework vibrations associated with the M_3C core of the above ketenylidene clusters are reported. Assignments were made with the aid of Raman depolarization ratio measurements on samples in CH_2Cl_2 solution and in some cases on polycrystalline solids.

Introduction

Ligands attached to metal clusters are useful structural models for similar species on metal surfaces,[1] and the spectroscopic fingerprints of these ligands in structurally characterized metal clusters are useful for the identification of surface species. For example, alkyl and vinyl fragments have been detected on metal surfaces by the correspondence of vibrational spectra of surfaces to spectra of the metal cluster analogues.[1b,2]

The ready conversion of carbide (C) and methylene (CH_2) to the CCO moiety in molecular clusters[3-5] suggests that a similar process may occur on metal surfaces that contain low-coordinate surface-bound carbide or methylene functionalities.[6] Although the μ_3-CCO ligand is stable on a variety of trimetallic group VIII transition-metal clusters with a range of electronic charges from -2 to +1,[3,4,7-14] the μ_3-CCO moiety has not been identified on metal surfaces. In order to extend the vibrational spectroscopic data on possible surface species, we have undertaken the characterization by infrared and Raman spectroscopy of the μ_3-CCO ligand in several metal clusters. A preliminary report of this work has appeared.[15]

(1) (a) Muetterties, E. L. *Pure Appl. Chem.* **1982**, *54*, 83. (b) Somorjai, G. A. *Chem. Soc. Rev.* **1984**, *13*, 321 and references contained therein.
(2) (a) Sheppard, N. *J. Electron Spectrosc.* **1986**, *38*, 175 and references contained therein. (b) Canning, N. D. S.; Madix, R. J. *J. Phys. Chem.* **1984**, *88*, 2437.
(3) Holmgren, J. S.; Shapley, J. R. *Organometallics* **1984**, *3*, 1322.
(4) Shapley, J. R.; Strickland, D. S.; St. George, G. M.; Churchill, M. R.; Bueno, C. *Organometallics* **1983**, *2*, 185.
(5) (a) Davis, J. H.; Beno, M. A.; Williams, J. M.; Zimmie, J.; Tachikawa, M.; Muetterties, E. L. *Proc. Natl. Acad. Sci. U.S.A.* **1981**, *78*, 668. (b) Bogdan, P. L.; Sabat, M.; Sunshine, S. A.; Woodcock, C.; Shriver, D. F. *Inorg. Chem.* **1988**, *27*, 1904.
(6) (a) Biloen, P.; Sachtler, W. M. H. *Adv. Catal.* **1981**, *30*, 165. (b) Kelley, R. D.; Goodman, D. W. In *The Chemical Physics of Solid Surfaces and Heterogeneous Catalysis*; King, D. A., Woodruff, D. P., Eds.; Elsevier: Amsterdam, 1982; p 427.
(7) Kolis, J. W.; Holt, E. M.; Shriver, D. F. *J. Am. Chem. Soc.* **1983**, *105*, 7307.
(8) Sailor, M. J.; Shriver, D. F. *Organometallics* **1985**, *4*, 1476.
(9) Went, M. J.; Sailor, M. J.; Bogdan, P. L.; Brock, C. P.; Shriver, D. F. *J. Am. Chem. Soc.*, in press.
(10) Kolis, J. W.; Holt, E. M.; Hriljac, J. A.; Shriver, D. F. *Organometallics* **1984**, *3*, 496.
(11) Crespi, A. M.; Shriver, D. F. *Organometallics* **1986**, *5*, 1750.
(12) Sailor, M. J.; Brock, C. P.; Shriver, D. F. *J. Am. Chem. Soc.*, in press.
(13) Seyferth, D.; Hallgren, J. E.; Eschbach, C. S. *J. Am. Chem. Soc.* **1974**, *96*, 1730.
(14) Mlekuz, M.; D'Agostino, M. F.; Kolis, J. W.; McGlinchey, M. J. *J. Organomet. Chem.* **1986**, *303*, 361.

0020-1669/88/1327-2666$01.50/0

Experimental Section

The compounds $[PPN]_2[Ru_3(CO)_6(\mu\text{-}CO)_3(\mu_3\text{-}CCO)]$,[12] $[PPN][HRu_3(CO)_9(\mu_3\text{-}CCO)]$,[12] $H_2Ru_3(CO)_9(\mu_3\text{-}CCO)$,[12] $[PPN]_2[Fe_3(CO)_9(\mu_3\text{-}CCO)]$,[7] $[PPN]_2[Os_3(CO)_9(\mu_3\text{-}CCO)]$,[9] and $[Co_3(CO)_9(\mu_3\text{-}CCO)][PF_6]$[13] and the ^{13}C isotopomers[12] of $[PPN]_2[Ru_3(CO)_6(\mu\text{-}CO)_3(\mu_3\text{-}CCO)]$ and $H_2Ru_3(CO)_9(\mu_3\text{-}CCO)$ were prepared according to published procedures (PPN = bis(triphenylphosphine)nitrogen(1+)). The extent and specificity of ^{13}C enrichments were checked by ^{13}C NMR spectroscopy. Infrared spectra were collected on samples in KBr or CsI pellets or Nujol mulls on KBr plates. Raman spectra were obtained on solid samples sealed under vacuum in 5-mm glass NMR tubes (Aldrich) or on solution samples prepared by vacuum transfer of CH_2Cl_2 onto the sample followed by sealing of the tube under vacuum. The CH_2Cl_2 solvent was distilled once from P_2O_5, vacuum distilled, and checked by GC for purity before use.

Infrared spectra were acquired on a Nicolet 7199 Fourier-transform infrared spectrometer or a Perkin-Elmer 283 grating infrared spectrometer. Cryogenic infrared spectra were obtained from samples cooled with liquid nitrogen in an evacuated cell with NaCl windows. Spectral resolution was 2 cm^{-1}.

Raman spectra were obtained with krypton laser excitation (6471 or 6764 Å) filtered by a premonochromator to remove laser plasma lines. Data were collected in a standard 180° backscattering geometry from spinning samples,[16] and the Raman scattered light was analyzed with a Spex 1401 double monochromator. The spectral resolution was varied subject to the desired resolution and signal-to-noise ratio required for the particular sample. The spectral band-pass was typically from 0.5 to 1 cm^{-1} for spectra obtained on solid samples in the CO stretching region. The natural line width of samples in solution was often ca. 10 cm^{-1}, and so the band-pass of the monochromator was set at 5 cm^{-1}. The polarization measurements were typically run with 8–10-cm^{-1} band-pass. Low-temperature Raman spectra were obtained in an optical cryostat that has been described previously.[16b] Raman shifts reported are accurate to ±2 cm^{-1}.

Raman polarization data were collected on stationary solution samples and spinning solid samples with use of a backscattering geometry,[16c] for which depolarized (non totally symmetric) bands have $\rho = {}^3/_4$ and totally symmetric bands have the theoretical range $0 \leq \rho \leq {}^3/_4$. Standard checks of the accuracy of the technique were made on the 459-, 314-, and 218-cm^{-1} lines of CCl_4.[17] Additionally the ν_4 (A_1) band of CH_2Cl_2 at 288 cm^{-1} ($\rho = 0.30$)[17c] served as an internal standard for the polarization measurements of solution samples.

Depolarization ratios were calculated by the subtraction technique described below. Since the depolarization ratio ρ of a given peak is related to $I_\perp$ and $I_\parallel$ by

$$\rho = \frac{I_\perp}{I_\parallel} \tag{1}$$

a difference spectrum that is scaled by a factor R defined as

$$I_{diff} = I_\perp - RI_\parallel \tag{2}$$

is related to the depolarization ratio by

$$I_{diff} = I_\parallel(\rho - R) \tag{3}$$

Thus, R was adjusted in a spectral subtraction program to null the intensity of the peak being measured with respect to the base line. At this point I_{diff} in eq 3 becomes equal to zero and the subtraction factor R is equal to the depolarization ratio ρ for that peak.

Results and Discussion

Vibrations Associated with the CCO Moiety. The ketenylidene cluster $[Ru_3(CO)_6(\mu\text{-}CO)_3(\mu_3\text{-}CCO)]^{2-}$ (anion of **1**) was chosen for detailed study because its crystal structure is known[8] and previous work has shown that **1** can be selectively ^{13}C enriched at either or both carbon atoms of the CCO ligand.[12] The symmetry of $[PPN]_2[Ru_3(CO)_6(\mu\text{-}CO)_3(\mu_3\text{-}CCO)]$ in the solid state is approximately C_{3v}, with a set of three bridging CO ligands lying roughly in the plane of the metals and two sets of three terminally bound CO ligands arranged above and below the plane of the metals.[8] The C–C and C–O bond distances of the symmetrically capping CCO group of **1** (Figure 1) are essentially the same as those of $H_2C{=}C{=}O$ (1.31 (1) vs 1.30 (1) Å and 1.16 (1) vs 1.17 (1) Å for the C=C and C=O bonds of H_2CCO and **1**, respectively[18]); therefore, it is not surprising that the vibrational signatures of **1** and ketene are similar. There are two stretching vibrations associated with the CCO group. In this discussion the high-frequency CCO stretching component will be referred to as ν_1 while ν_2 will refer to the low-frequency CCO stretch.

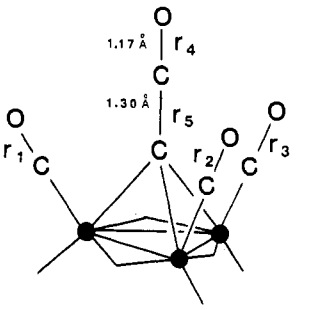

Figure 1. Disposition of the μ_3-CCO ligand in $[PPN]_2[Ru_3(CO)_6(\mu\text{-}CO)_3(\mu_3\text{-}CCO)]$ showing the internal coordinates used in the normal-coordinate analysis. Bond distances are taken from the X-ray crystal structure.[8]

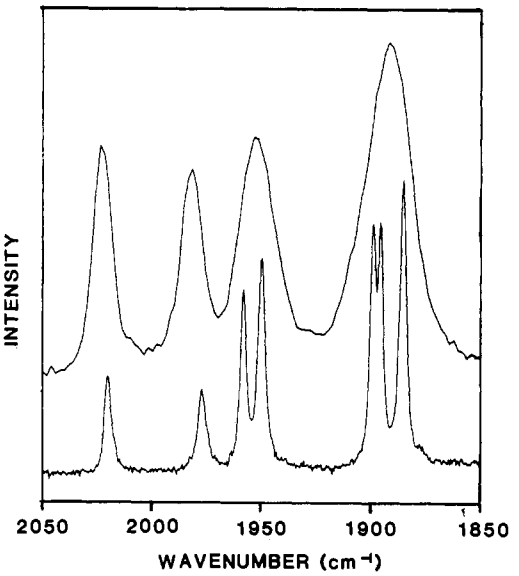

Figure 2. Raman spectra of $[PPN]_2[Ru_3(CO)_6(\mu\text{-}CO)_3(\mu_3\text{-}CCO)]$ in the terminal ν_{CO} region of solid (lower) and CH_2Cl_2 solution (upper) samples. The two highest frequency vibrations are polarized for Raman spectra on solutions.

In solid $[PPN]_2[Ru_3(CO)_6(\mu\text{-}CO)_3(\mu_3\text{-}CCO)]$ the site symmetry of the metal cluster in the unit cell is C_1, and there is a single metal cluster molecule per asymmetric unit.[8] Therefore, in principle all degeneracies of the C_{3v} point group should be removed in the vibrational spectra of crystalline **1**, and the maximum expected number of ν_{CO} bands for the terminal carbonyls is 6. However, the Raman spectrum of **1** in the solid state, presented in Figure 2, shows that there are seven bands in the terminal CO stretching region. Spectra of **1** that had been isotopically substituted at the CCO with ^{13}C firmly establish that the ν_1 vibration of CCO also occurs in this region, thus accounting for the extra vibrational band observed. Figure 3 shows the infrared spectra of two samples of $[PPN]_2[Ru_3(CO)_6(\mu\text{-}CO)_3(\mu_3\text{-}CCO)]$ in the carbonyl region, the solid line representing a sample of **1** that is ^{13}C-enriched at the CCO ligand (80% at C_α and 50% at C_β of $C_\alpha C_\beta O$) and the dotted line representing **1** at natural abundance. From Figure 3 it is apparent that the two highest frequency bands

(15) Sailor, M. J.; Shriver, D. F. *J. Am. Chem. Soc.* **1987**, *109*, 5039.
(16) (a) Strommen, D. P.; Nakamoto, K. *Laboratory Raman Spectroscopy*; Wiley: New York, 1984. (b) *Ibid.*, p 57. (c) *Ibid.*, p 88. (d) *Ibid.*, p 91.
(17) (a) Murphy, W. F.; Evans, M. V.; Bender, P. *J. Chem. Phys.* **1967**, *47*, 1836. (b) Douglas, A. E.; Rank, D. H. *J. Opt. Soc. Am.* **1948**, *38*, 281. (c) Long, D. A. *Raman Spectroscopy*; McGraw-Hill: New York, 1977; p 143.
(18) Cox, A. P.; Thomas, L. F.; Sheridan, J. *Spectrochim. Acta* **1959**, *15*, 542.

Table I. Observed Vibrational Frequencies (cm^{-1}) for $[PPN]_2[Ru_3(CO)_6(\mu\text{-}CO)_3(\mu_3\text{-}CCO)]$ ^{13}C-Enriched at the μ_3-CCO Ligand[a]

CCO		$^{13}C^{13}CO$[b]		^{13}CCO[c]	
IR	Raman	IR	Raman	IR	Raman
2022 (m)	2020 (w)	2019 (w)	2018 (w)	2019 (m)	2016 (w)
			2007 (w)		
1977 (s)	1977 (w)	1976 (m)	1975 (vw)	1975 (s)	1973 (w)
1959 (s)	1958 (m)	1960 (s)	1959 (m)	1960 (m, sh)	1957 (m)
1952 (vs)	1950 (m)	1952 (vs)	1951 (m)	1952 (vs)	1950 (m)
1942 (s, sh)		1943 (s)		1945 (vs)	
		1935 (vs)	1936 (vw)	1921 (m)	1923 (vw)
1901 (s)	1899 (s)	1901 (s, sh)	1898 (s)	1901 (s, sh)	1899 (s)
1897 (s)	1895 (s)	1897 (s)	1895 (s)	1897 (s)	1895 (s)
1889 (m)	1885 (vs)	1889 (m)	1885 (vs)	1891 (m)	1885 (vs)
1789 (vw)	1792 (s)	1789 (vw)	1792 (s)	1802 (vw)	1792 (s)
1743 (s)	1751 (vw)	1743 (s)	1751 (vw)	1743 (s)	1750 (vw)
1735 (s)		1734 (s)		1734 (s)	
	1309 (vw)		1309 (vw)		1309 (vw)
			1277 (vw)		1277 (vw)
			1271 (vw)		
	321 (s)		317 (s)		319 (s)
	270 (m)[d]		270 (m)[d]		268 (m)[d]
	242 (m, br)[d]		240 (m, br)[d]		242 (m, br)[d]
	205 (vs)		204 (vs)		204 (vs)
	178 (w)[d]		178 (w)[d]		179 (w)[d]
	153 (m)		152 (m)		152 (m)

[a] Bands associated with the counterion or those insensitive to ^{13}C substitution of the CCO are reported in the supplementary material. [b] Sample is ^{13}C-enriched 80% at C_α and 50% at C_β of $C_\alpha C_\beta O$. [c] Sample is ^{13}C-enriched 50% at C_α of $C_\alpha C_\beta O$. [d] Present in the [PPN]Cl spectrum.

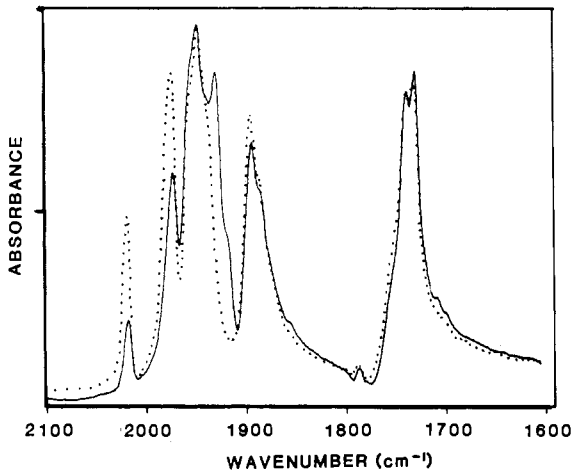

Figure 3. Infrared spectra (absorbance mode) of solid $[PPN]_2[Ru_3(CO)_6(\mu\text{-}CO)_3(\mu_3\text{-}CCO)]$ (dotted line) and $[PPN]_2[Ru_3(CO)_6(\mu\text{-}CO)_3(\mu_3\text{-}*C*CO)]$ (solid line) in KBr. The latter sample is enriched exclusively at the μ_3-$C_\alpha C_\beta O$ ligand (80% at C_α, 50% at C_β).

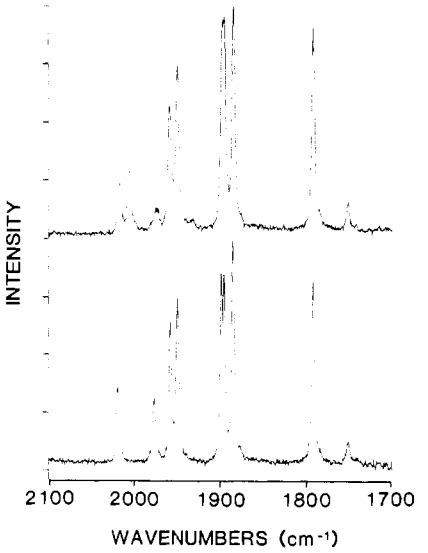

Figure 4. Raman spectra of solid $[PPN]_2[Ru_3(CO)_6(\mu\text{-}CO)_3(\mu_3\text{-}CCO)]$ (lower) and $[PPN]_2[Ru_3(CO)_6(\mu\text{-}CO)_3(\mu_3\text{-}*C*CO)]$ (upper). The latter sample contains the label exclusively at the $C_\alpha C_\beta O$ ligand (80% at C_α, 50% at C_β).

are affected by isotopic substitution of the CCO. The 2020- and 1977-cm^{-1} bands are reduced in intensity, and a new band at 1936 cm^{-1} is apparent in the infrared spectrum of the ^{13}C-enriched sample. Presumably the 1936-cm^{-1} band is the ^{13}C isotopic counterpart of the 1977-cm^{-1} band. Although it could not be resolved in the infrared spectrum, the isotopic frequency corresponding to the 2020-cm^{-1} band is evident in the Raman spectrum at 2007 cm^{-1} (Figure 4). Since both the 1977- and the 2020-cm^{-1} bands (assigned to ν_1 of the CCO and ν_{CO} of the metal-bound carbonyls, respectively) shift on isotopic substitution of CCO, it is concluded that a significant degree of vibrational coupling exists between the CCO unit and the metal-bound carbonyls. Mixing of the two bands is not restricted by symmetry, because the 2020- and 1977-cm^{-1} peaks are found to be polarized in the Raman spectrum, indicating that they both belong to A_1-symmetry vibrations (depolarization ratios in solution of 0.56 and 0.51 ± 0.04, respectively).

The frequency of ν_1 for the ketenylidene cluster **1** is typical of the CCO stretching frequencies found for a variety of related organometallic ketene compounds.[19,20] It is usually easy to assign this vibration in metal-substituted ketenes that contain only one or two other CO ligands. For instance, in the series of complexes $CpM(CO)_{3-x}(PMe_3)_x[C(CO)R]$ (M = Mo, W; x = 1,2) the ketene CO stretch ranges from 1990 to 2030 cm^{-1} while the metal-bound CO stretch appears in a lower energy region, from 1760 to 1950 cm^{-1}.[19]

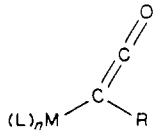

(19) Uedelhoven, W.; Eberle, K.; Kreissl, F. R. *Chem. Ber.* **1979**, *112*, 3376.

(20) (a) Casey, C. P.; Fagan, P. J.; Day, V. W. *J. Am. Chem. Soc.* **1982**, *104*, 7360. (b) Paiaro, G.; Pandolfo, L. *Angew. Chem., Int. Ed. Engl.* **1981**, *20*, 288. (c) Paiaro, G.; Pandolfo, L. *Angew. Chem., Int. Ed. Engl.* **1981**, *20*, 289. (d) Martin-Gil, J.; Howard, J. A. K.; Navarro, R.; Stone, F. G. A. *J. Chem. Soc., Chem. Commun.* **1979**, 1168. (e) Hillhouse, G. L. *J. Am. Chem. Soc.* **1985**, *107*, 7772.

(21) Wilson, E. B.; Decius, J. C.; Cross, P. C. *Molecular Vibrations*; McGraw-Hill: New York, 1965.

Table II. Frequencies Assigned to the ν_2 Component of CCO in μ_3-CCO Clusters

compd	ν_2, cm^{-1}
$[PPN]_2[Ru_3(CO)_6(\mu\text{-}CO)_3(\mu_3\text{-}CCO)]$	1309[a,b]
$[PPN]_2[Fe_3(CO)_9(\mu_3\text{-}CCO)]$	1342[a,c]
$H_2Ru_3(CO)_9(\mu_3\text{-}CCO)$	1256[d,e]
$[Co_3(CO)_9(\mu_3\text{-}CCO)][PF_6]$	1211[d,f]

[a] Raman measurement. [b] Shifts to 1277 cm^{-1} in ^{13}CCO isotopomer. [c] Tentative assignment. [d] IR measurement. [e] Shifts to 1230 cm^{-1} in ^{13}CCO isotopomer. [f] Hydrolysis of sample leads to disappearance of 1211-cm^{-1} band and appearance of bands characteristic of $Co_3(CO)_9(\mu_3\text{-}CC(O)OH)$.

The low-frequency CCO stretching component of **1**, referred to here as ν_2, is assigned to a weak band appearing in the Raman spectrum at 1309 cm^{-1} that shifts to lower frequency in the ^{13}C-substituted species (Table I). Table II lists the values of the frequencies assigned to ν_2 for several other ketenylidene clusters. In some cases ν_2 is more easily observed in the Raman spectrum than in the infrared spectrum because of the presence of strong infrared-active vibrations from the counterions. In all of the clusters studied, ν_2 appears in the region from 1200 to 1350 cm^{-1}. This stretch distinguishes the CCO group from metal-bound CO ligands, which do not have vibrational frequencies in this region, although it is difficult to observe ν_2 in IR and Raman spectra because of its low intensity. The ν_2 vibration appears to decrease in frequency with increasing positive charge on the cluster (Table II).

Approximate Normal-Coordinate Analysis. The Wilson **F** and **G** matrix method[21] was used to analyze the form of the secular equation responsible for the CCO vibrations of $[PPN]_2[Ru_3(CO)_6(\mu\text{-}CO)_3(\mu_3\text{-}CCO)]$ and to fit the isotopic data on the CCO stretching vibrations of **1** to an approximate force field. A simplified valence force field involving five internal bond stretching coordinates was employed, corresponding to three metal-bound symmetry-related CO bonds (r_1, r_2, and r_3) and the C–O and C–C bonds of the CCO ligand (r_4 and r_5) (see Figure 1). The metal-bound CO groups are included in order to model the mixing of the ν_1 vibration of the CCO unit with a metal carbonyl vibration. Assuming the point group C_{3v}, the symmetry coordinates chosen for the preceding arrangement are

A_1 symmetry

$$s_1 = 1/3^{1/2}\,(r_1 + r_2 + r_3)$$

$$s_2 = r_4$$

$$s_3 = r_5$$

E symmetry

$$s_4 = 1/6^{1/2}\,(2r_1 - r_2 - r_3)$$

$$s_5 = 1/2^{1/2}\,(r_2 - r_3)$$

Since we were primarily concerned with the CCO stretching modes, which are of A_1 symmetry, the analysis was restricted to the A_1 symmetry block. It has been pointed out that CO oscillator interactions can occur by either a through-space (dipole–dipole) or through-bond ("vibronic") coupling mechanism and that either of these phenomena result in the same form of the secular determinant.[22] Thus, the model used in the present calculation assumes no particular mechanism and no assumption is made about the geometric disposition of the metal-bound CO ligands, other than the fact that they are symmetry related through the point group C_{3v} and the CCO ligand lies on the C_3 axis of the system.

The A_1 block of the symmetry-factored secular determinant was derived by standard methods.[21] The nine observed data for the $^{12}C^{12}CO$, $^{13}C^{12}CO$, and $^{13}C^{13}CO$ isotopomers of $[PPN]_2[Ru_3(CO)_6(\mu\text{-}CO)_3(\mu_3\text{-}CCO)]$ were fit to the secular equation with the aid of a nonlinear least-squares fitting routine.[23] Observed and calculated results are given in Table III. For **1** there are two alternative solutions to the secular determinant differing only in the relative signs of the interaction force constants f_{12} and f_{13}. On the basis of analogy to CO interaction constants in metal carbonyl cluster systems,[26] the (metal) CO to (ketenyl) CO interaction constant f_{12} was taken as positive, necessitating that the (metal) CO to (ketenyl) CC interaction constant f_{13} be negative. The force constants obtained from the least-squares fit of the data are listed in Table IV.

Table III. Observed and Calculated CCO Stretching Frequencies (cm^{-1}) for $[PPN]_2[Ru_3(CO)_6(\mu\text{-}CO)_3(\mu_3\text{-}CCO)]$, H_2CCO, and Free CCO

	$[PPN]_2[Ru_3(CO)_6(\mu\text{-}CO)_3(\mu_3\text{-}CCO)]$[a]				
	$^{12}C^{12}CO$	$^{13}C^{12}CO$	$^{13}C^{13}CO$	H_2CCO[b]	CCO[c]
obsd	2020	2016	2007		
calcd	2019	2018	2006		
obsd	1977	1973	1936	2152	1978
calcd	1976	1975	1935	2155	1978
obsd	1309	1277	1271	1118	1075
calcd	1310	1275	1272	1129	1075

[a] Observed frequencies are Raman data. [b] Observed and calculated data obtained from ref 24. [c] Observed data obtained from ref 25.

Table IV. Derived Force Constants (N m^{-1}) for CCO[a]

force constant	**1**	H_2CCO[b]	CCO[c]
f_1	1615		
f_2	1644	1611	1475
f_3	891	862	623
f_{23}	316	96	122
f_{12}	14		
f_{13}	8		

[a] Force constant definitions: f_1 is the "effective" C–O force constant for the metal-bound CO ligands on **1** (ignoring other metal–carbonyl interactions); f_2 and f_3 are the C–O and C–C force constants, respectively, of the CCO moiety; f_{xy} values are the interaction force constants between f_x and f_y. [b] Data taken from ref 24. [c] Force constants derived from vibrational data from ref 25 (see text).

Table V. Potential Energy Distribution in the Valence Coordinates of the CCO Stretching Modes of $[PPN]_2[Ru_3(CO)_6(\mu\text{-}CO)_3(\mu_3\text{-}CCO)]$ (**1**) and Matrix-Isolated CCO[a]

	$\nu_{CO}(1)$	$\nu_1(1)$	$\nu_1(CCO)$[b]	$\nu_2(1)$	$\nu_2(CCO)$[b]
freq, cm^{-1}	2020	1977	1978	1309	1075
$r_{1-3}(MC{\equiv}O)$	49	39		0	
$r_4(C{=}O)$	39	47	81	10	13
$r_5(C{=}C)$	12	14	19	90	87

[a] r_{1-3}, r_4, and r_5 are the metal C–O, ketenyl C–O, and ketenyl C–C valence coordinates, respectively, as described in the text. [b] Frequency data from ref 24.

The vibrational data on matrix-isolated $^{12}C^{12}C^{16}O$, $^{13}C^{12}C^{16}O$, $^{12}C^{13}C^{16}O$, and $^{12}C^{12}C^{18}O$ obtained from ref 25 were fit to a valence force field model similar to the one employed for $[PPN]_2[Ru_3(CO)_6(\mu\text{-}CO)_3(\mu_3\text{-}CCO)]$, and the values of f_2, f_3, and f_{23} were refined by using the same vibrational analysis program.[23] The force field reported in Table IV, the potential energy distribution of Table V, and the form of the normal modes for free CCO of Figure 5 are derived from the present analysis. For H_2CCO, the vibrational data listed in Table III as well as the calculated force field elements of Table IV were taken directly from ref 24.

(22) Haas, H.; Sheline, R. K. *J. Chem. Phys.* **1967**, *47*, 2996.
(23) Program QCMPO12, Quantum Chemistry Program Exchange; Indiana University: Bloomington, IN.
(24) Moore, C. B.; Pimentel, G. C. *J. Chem. Phys.* **1963**, *38*, 2816.
(25) Jacox, M. E.; Milligen, D. E.; Moll, N. G.; Thompson, W. E. *J. Chem. Phys.* **1965**, *43*, 3734.
(26) Sutton, L. E., Ed. *Tables of Interatomic Distances and Configuration in Molecules and Ions*; The Chemical Society: London, 1958.

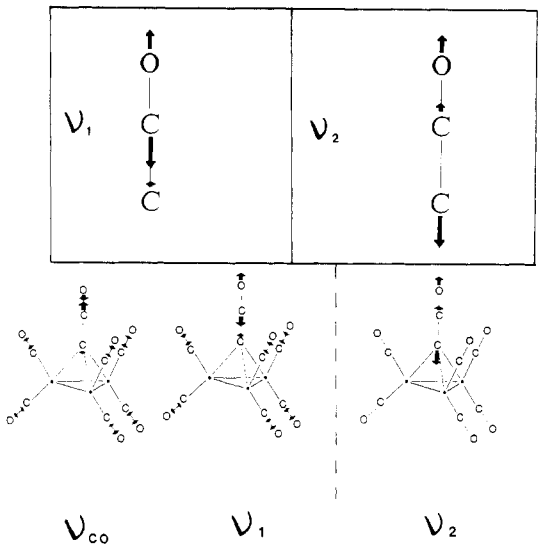

Figure 5. Comparison of the forms of the normal modes for the CCO stretching vibrations of matrix-isolated CCO (upper) and $[PPN]_2[Ru_3(CO)_6(\mu\text{-}CO)_3(\mu_3\text{-}CCO)]$ (lower). Coupling of the CCO with metal carbonyls gives rise to the two high-frequency vibrations for $[PPN]_2[Ru_3(CO)_6(\mu\text{-}CO)_3(\mu_3\text{-}CCO)]$ designated ν_{CO} and ν_1.

Vibrational Potential Function of the CCO in $[Ru_3(CO)_6(\mu\text{-}CO)_3(\mu_3\text{-}CCO)]^{2-}$. As shown in Table III, there is good agreement between the nine observed vibrational frequencies for the $^{12}C^{12}CO$, $^{13}C^{12}CO$, and $^{13}C^{13}CO$ isotopomers of $[PPN]_2[Ru_3(CO)_6(\mu\text{-}CO)_3(\mu_3\text{-}CCO)]$ and those calculated from the six-parameter force field. Although approximate, the analysis leads to reasonable force constants in comparison to other systems. For example, the primary force constants f_2 and f_3 for the CCO ligand of **1** are comparable to those of H_2CCO.[24]

The frequencies for ν_2 in the ketenylidene clusters are ca. 100–200 cm^{-1} higher and the frequencies for ν_1 are ca. 200 cm^{-1} lower than the corresponding vibrations in H_2CCO.[24] The normal-coordinate analysis of $[PPN]_2[Ru_3(CO)_6(\mu\text{-}CO)_3(\mu_3\text{-}CCO)]$ indicates that the large interaction force constant between CC and CO of the CCO partially accounts for this difference. For example, the primary CC and CO force constants for H_2CCO[24] and $[PPN]_2[Ru_3(CO)_6(\mu\text{-}CO)_3(\mu_3\text{-}CCO)]$ are essentially the same but the interaction constant f_{23} is 3 times larger in the ketenylidene cluster than in ketene.[24] The effect of the interaction force constant f_{23} on the frequencies of ν_1 and ν_2 is shown in Figure 6. When the primary CC and CO force constants f_2 and f_3 are held constant, the frequency calculated for ν_1 decreases and that for ν_2 increases on increasing f_{23} from 0.0 to 400 N m^{-1}.

The positive value of the interaction constant f_{23} of **1** indicates that when the C–C bond of the CCO is lengthened the strength of the C–O bond increases and, similarly, when the C–C vector shortens the C–O bond strength decreases. Thus, the interaction force constant can be thought of as a measure of the accessibility of resonance forms B and C. In this interpretation the effect of

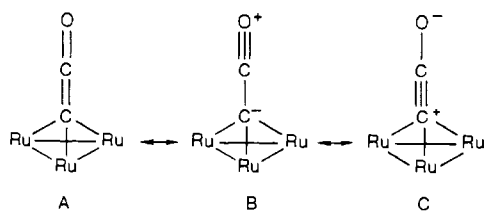

shortening the C–O bond is to favor resonance structure B, and therefore the C–C bond is weakened. Likewise the effect of lengthening the C–O bond is to favor resonance structure C. An analogous description has been presented for the vibrational potential function of CO_2.[21] Similarly, Moore et al. noted that the large interaction constant for ketene may reflect the energy stabilization afforded by resonance forms of H_2CCO.[24] The much larger interaction force constant calculated for the CCO of **1** than for ketene indicates that a greater amount of valence reorganization occurs in the CCO vibrations of $[PPN]_2[Ru_3(CO)_6(\mu\text{-}CO)_3(\mu_3\text{-}CCO)]$ than in ketene. Apparently the resonance forms of CCO represented by B and C are more readily accommodated in the triruthenium cluster. This may be a reflection of the ability of the trimetal framework to stabilize the valence isomers of C=C=O by acting as an electron reservoir for the CCO ligand.

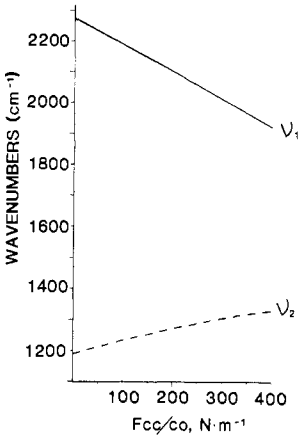

Figure 6. Calculated effect of the CC to CO interaction force constant (f_{23} in the present work) on the frequencies of ν_1 and ν_2 modes of a CCO molecule. The carbon–carbon and carbon–oxygen force constants f_3 and f_2 were held at 891 and 1644 N m^{-1}, respectively.

The primary C–C force constant for the CCO in $[PPN]_2[Ru_3(CO)_6(\mu\text{-}CO)_3(\mu_3\text{-}CCO)]$, at 891 N m^{-1}, is smaller than typical alkene C=C stretching force constants, which range from 950 to 990 N m^{-1}.[21] Additionally the primary C–O force constant for the CCO in **1**, at 1644 N m^{-1}, is larger than standard ketonic C=O stretching force constants, which range from 1180 to 1340 N m^{-1}.[21] The force constants for **1** seems to indicate that valence form B contributes to the ground-state bonding in **1**, because this would account for the relatively weak C–C and relatively strong C–O bonds. The ^{13}C NMR data for **1** lends support to this postulate. The chemical shift of C_α in the C_α–C_β–O ligand of **1** is at an extremely high field position, −28.3 ppm with respect to TMS, indicating that C_α is highly shielded.[8] Although the above arguments might suggest that the C–C bond in **1** should be longer than a typical double bond, the C–C bond distance of the CCO in **1**, 1.30 (1) Å,[8] is actually slightly shorter than the standard double-bond distance of 1.337 (6) Å.[26]

Apart from the coupling between the two CCO stretching vibrations, it is apparent from the spectra of the isotopomers of **1** that the CCO unit is also vibrationally coupled to the metal-bound carbonyls. The mixing of the CCO stretches with a terminal CO vibration is somewhat analogous to the coupling between CO ligands on separate metal centers observed in carbonyl clusters. Detailed vibrational analyses of polynuclear clusters have shown that the interaction of carbonyl groups on adjacent metal centers can be as large as the interaction between CO ligands on the same metal.[27] As a consequence, it is often inadequate to use a local-symmetry approach in the interpretation of cluster carbonyl spectra. In a valence force field analysis, interactions of CO oscillators are modeled by the introduction of off-diagonal elements in the force field matrix. Geminal (on the same metal) and vicinal (through the M–M bond) interaction force constants have been introduced to account for vibrational communication between CO groups on metal clusters.[27] The interaction force constants in metal carbonyl clusters are typically 0–2% in the primary C–O force constant, and generally the geminal interactions are larger than the longer range vicinal couplings.[27] In the force field calculated for $[PPN]_2[Ru_3(CO)_6(\mu\text{-}CO)_3(\mu_3\text{-}CCO)]$, the interaction force constant f_{12} responsible for the coupling of the metal-bound CO

(27) (a) Battiston, G. A.; Bor, G.; Dietler, U. K.; Kettle, S. F. A.; Rossetti, R.; Sbrignadello, G.; Stanghellini, P. L. *Inorg. Chem.* **1980**, *19*, 1961. (b) Bor, G.; Sbrignadello, G.; Marcati, F. *J. Organomet. Chem.* **1972**, *46*, 357. (c) Bor, G.; Sbrignadello, G.; Noack, K. *Helv. Chim. Acta* **1975**, *58*, 815. (d) Moskovits, M.; Hulse, J. E. *Surf. Sci.* **1978**, *78*, 397 and references contained therein.

Table VI. $M_3(\mu_3\text{-CCO})$ Core Vibrations (cm^{-1}) and Depolarization Ratios[a]

compd	M_3–C (A_1)		M–M (A_1)		M–M (E)	
	ν	ρ	ν	ρ	ν	ρ
$[Ru_3(CO)_9(\mu_3\text{-CCO})]^{2-}$	319	0.12 (2)	206	0.19 (2)	154	0.7 (1)
$[HRu_3(CO)_9(\mu_3\text{-CCO})]^-$	320	0.25 (5)	209	0.21 (1)	172	0.7 (1), 0.4 (1)[c]
$H_2Ru_3(CO)_9(\mu_3\text{-CCO})$[b]	338		205		174	
$[Os_3(CO)_9(\mu_3\text{-CCO})]^{2-}$	359	0.2 (1)	179	0.21 (2)	142	0.78 (3)
$[Fe_3(CO)_9(\mu_3\text{-CCO})]^{2-}$	332	0.16 (3)	215	0.18 (2)	179	0.75 (2)
$[Fe_3(CO)_9(\mu_3\text{-CCO})]^{2-}$[b]	334	0.40 (5)	215	0.43 (2)	181	0.70 (5), 0.55 (5)[c]
$[Co_3(CO)_9(\mu_3\text{-CCO})]^+$[b]	357	0.45 (5)	209	0.52 (5)	176	0.7 (1)

[a] All samples run in CH_2Cl_2 solution unless otherwise noted. The counterion for the anions is $[PPN]^+$; the counterion for the cationic cluster is $[PF_6]^-$. Errors quoted are 95% confidence limits. [b] Crystalline sample. [c] Asymmetric peak.

ligands with CO of the CCO is 14 N m^{-1}, which is in the same range as the vicinal interaction force constants observed on $Ru_3(CO)_{12}$ (range 12.5–20.8 N m^{-1}).[27a] However, it should be pointed out that in the present analysis the choice of the algebraic sign of f_{12} is arbitrary and so the apparent similarity to the force constants of $Ru_3(CO)_{12}$ may not be real.

The above normal-coordinate model gives a good representation of the vibrational frequenies of the various isotopomers and provides a sensible representation of the portion of the eigenvectors associated with the CCO ligand. However, it does not furnish a full representation of the form of the metal-bound CO stretching coordinates. Although it is not a significant issue in the present study, we note for the sake of completeness that a symmetric in-phase CO stretch for the metal-bound CO ligands is the best approximation for the CO oscillators coupled to CCO. This concept is incorporated into Figure 5.

Cluster Framework Vibrations. A symmetrical capping CCO ligand on a trimetallic equilateral triangle has C_{3v} symmetry. Under this point group there are eight normal modes associated with the $M_3(\mu_3\text{-CCO})$ unit, four of A_1 symmetry and four doubly degenerate E-symmetry modes. Two of the A_1-symmetry modes, the CCO-associated stretches ν_1 and ν_2, have just been discussed. The other two totally symmetric modes and one of the E-symmetry modes responsible for the metal–carbon and metal–metal stretches can be readily assigned on the basis of Raman measurements. Because they involve motions of the heavy and highly polarizable metal atoms, these vibrations all give rise to strong bands in the low-frequency region of the Raman spectrum. Table VI gives the low-energy vibrations and their measured depolarization ratios for several ketenylidene clusters. The two lowest frequency vibrations are, in approximate terms, the symmetric and antisymmetric metal–metal stretches, while the vibration around 300–350 cm^{-1} is assigned to the symmetric metal–carbon stretch corresponding to motion of the CCO unit along the molecular C_3 axis. Isotopic substitution of the CCO ligand of $[PPN]_2[Ru_3(CO)_6(\mu\text{-CO})_3(\mu_3\text{-CCO})]$ helps corroborate this assignment, as the peak maximum of the 321-cm^{-1} band of **1** shifts to a slightly lower frequency in the $^{13}C^{13}CO$ isotopomer (ca. 4 cm^{-1} for **1** enriched to 80% at *CCO and 50% at C*CO positions). Qualitatively the low-frequency spectra of these ketenylidene cluster compounds match those seen for other trinuclear metal clusters with capping C–R groups. Detailed vibrational studies have been performed on the clusters $Co_3(CO)_9(\mu_3\text{-CR})$ (R = H,[28] CH_3,[29] F,[30] Cl,[30] and Br[30]) and $H_3Ru_3(CO)_9(\mu_3\text{-CR})$ (R = H, Cl),[31] and in the cases where R ≠ H the symmetric (A_1) M–C stretch lies in the frequency range 250–400 cm^{-1} while the asymmetric (E) M–C stretch occurs at 550–650 cm^{-1}, ca. 250 cm^{-1} *higher* in energy than the symmetric counterpart.[29-31] The assignments were made on the basis of the relative intensities of these bands in the Raman and infrared spectra and the trends observed for several related compounds and were supported by normal-coordinate analyses.[29-31]

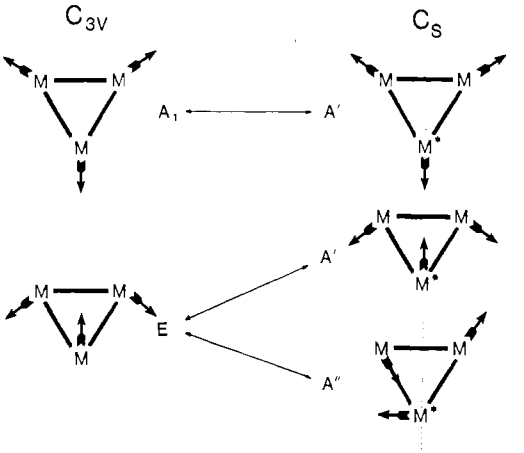

Figure 7. Correlation diagram for the reduction of C_{3v} to C_s symmetry. The metal–metal stretching vibrations for the trinuclear ketenylidene clusters are represented in approximate symmetry coordinates.

We have confirmed the assignment of the A_1-symmetry M–C stretch in the case of $Co_3(CO)_9(\mu_3\text{-CBr})$ by Raman depolarization ratio measurement ($\rho = 0.3 \pm 0.1$ for the 260-cm^{-1} band in CH_2Cl_2 solution). Similarly, Raman polarization data conclusively establish the 300–350-cm^{-1} band observed in the ketenylidene clusters to be of A_1 symmetry ($\rho < 3/4$; see Table VI). Assuming a force field analogous to that of the $Co_3(CO)_9(\mu_3\text{-CR})$ clusters, the M–C stretch of E symmetry should occur between 500 and 700 cm^{-1}. As none of the bands observed in the infrared or Raman spectra in this region are affected by isotopic substitution of the CCO ligand on $[PPN]_2[Ru_3(CO)_6(\mu\text{-CO})_3(\mu_3\text{-CCO})]$, we were unable to substantiate this prediction. The results of the Raman polarization measurements also establish the assignment of the metal–metal-associated stretches as $A_1 > E$ (or in the case of the clusters of C_s symmetry $A' > (A'' + A')$; Table VI).

Because multiple reflections in polycrystalline samples depolarize the incident laser light, depolarization ratio measurements are usually restricted to gas, liquid, or single-crystal samples. However, Strommen and Nakamoto have shown that approximate depolarization ratios can be obtained from polycrystalline solids when the sample is highly colored and, therefore, penetration of the sample by the laser is minimized.[16d] The dark color of some of the ketenylidene clusters in the present study allowed the collection of meaningful polarization data on polycrystalline samples. For instance, the two M_3C framework modes of $[PPN]_2[Fe_3(CO)_9(\mu_3\text{-CCO})]$ known from the solution studies to be highly polarized also had depolarization ratios that were significantly less than 3/4 in Raman spectra of the solid. Semiquantitative ρ's were also measured on the dark polycrystalline compound $[Co_3(CO)_9(\mu_3\text{-CCO})][PF_6]$ (see Table VI).

Sensitivity of the M–M Stretches to Molecular Symmetry. Typically two strong bands are observed in the 100–250-cm^{-1} region of the vibrational spectra of the trinuclear ketenylidene clusters. These correspond to the A_1- and E-symmetry metal–metal stretching vibrations expected for a molecular symmetry of C_{3v}, as depicted in Figure 7. For some of these compounds the assignment to C_{3v} symmetry is only approximate; for instance the compounds $[(\mu\text{-H})Ru_3(CO)_9(\mu_3\text{-CCO})]^-$ and $(\mu\text{-H})_2Ru_3(CO)_9(\mu_3\text{-CCO})$ contain hydride groups bridging metal–metal

(28) Howard, M. W.; Kettle, S. F.; Oxton, I. A.; Powell, D. B.; Sheppard, N.; Skinner, P. *J. Chem. Soc., Faraday Trans. 2* **1981**, *77*, 397.
(29) Skinner, P.; Howard, M. W.; Oxton, I. A.; Kettle, S. F. A.; Powell, D. B.; Sheppard, N. *J. Chem. Soc., Faraday Trans. 2* **1981**, *77*, 1203.
(30) Howard, M. W.; Oxton, I. A.; Powell, D. B.; Skinner, P. *Spectrochim. Acta, Part A* **1981**, *37A*, 473.
(31) Oxton, I. A. *Spectrochim. Acta, Part A* **1982**, *38A*, 181.

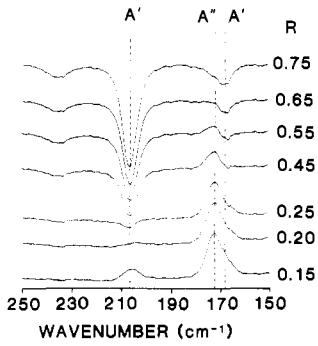

Figure 8. Determination of depolarization ratios of the Ru–Ru stretches of $[PPN][HRu_3(CO)_9(\mu_3\text{-}CCO)]$ by difference spectra. For a given peak, the value of R is equal to the depolarization ratio ρ when the peak is nulled with respect to the base line (see Experimental Section).

bonds and are strictly of C_s symmetry.[12] However, the effect of a bridging hydride on the M–M stretching vibrations is negligible in these complexes. Only slight asymmetry is observed in the E vibration, corresponding to a splitting of the degeneracy into its A′ and A″ components under the reduced symmetry type (see Figure 7). Careful examination of the polarized solution Raman spectra of $[PPN][HRu_3(CO)_9(\mu_3\text{-}CCO)]$ indicates that the depolarization ratio of the asymmetric E vibration varies over the width of the band. On the high-frequency side ρ is approximately 0.7, while on the low-frequency side ρ is ca. 0.4 (Figure 8). Apparently the difference in ρ across the band is a reflection of the splitting of this E mode caused by the presence of the μ-hydride into the symmetric A′ ($\rho \approx 0.4$) and antisymmetric A″ ($\rho \approx {}^3/_4$) bands of the C_s symmetry group.

Similarly, the solids $[PPN]_2[Fe_3(CO)_9(\mu_3\text{-}CCO)]$ and $[PPN]_2[Os_3(CO)_9(\mu_3\text{-}CCO)]$ were observed to have asymmetric M–M E modes. For the compound $[PPN]_2[Fe_3(CO)_9(\mu_3\text{-}CCO)]$ the E vibration splits into two distinct peaks at −90 °C. The splitting is not observed for the same sample in dichloromethane solution at −90 °C or in the $[Ph_4As]^+$ salt of $[Fe_3(CO)_9(\mu_3\text{-}CCO)]^{2-}$. The splitting observed in the $[PPN]^+$ salt is thus attributed to crystal-packing effects. The crystal structure of $[Ph_4As]_2[Fe_3(CO)_9(\mu_3\text{-}CCO)]$ shows that the CCO ligand is tilted toward a metal center,[7] but the lack of splitting of the E-symmetry vibration in the solid-state Raman spectrum of the $[PhAs_4]^+$ salt indicates that the M–M stretching modes are insensitive to this slight deviation from C_{3v} symmetry.

Possible Occurrence of CCO on Metal Surfaces. Given the precedent from metal cluster chemistry that conditions which generate low-coordinate carbide species tend to lead to CCO formation,[7-9] it is possible that metal surfaces with low-coordinate carbon atoms will also take on CO to form the CCO group.[15] Formation of a surface carbide species has been observed on a variety of metal surfaces.[6] For example, disproportionation of CO on an Ru(1,1,10) surface has been shown to produce a very active carbon species that can be removed as $C^{18}O$ under a stream of $^{18}O_2$.[32] Infrared studies of CO on carbided Ni and Co surfaces have been performed,[33] and EELS spectra of H_2CCO on Fe and Pt have been reported.[34] In these studies the possible occurrence of a μ_3-CCO species was not considered. It would be interesting to assess the role, if any, of CCO in surface chemistry. Indeed, it was mainly this aspect that inspired us to undertake the present study.

Assuming that CCO on a metal surface has a similar geometry and is subject to the analogous force field as on a metal cluster, it is clear that this species may be easily overlooked in the vibrational spectra of catalyst surfaces; the ν_1 stretch of CCO is in the same frequency region as metal carbonyl stretches, and the ν_2 stretch shows up in the same range as carbon–carbon bond stretching and carbon–hydrogen deformation vibrations.[2] Nevertheless, a feature of the CCO force field makes the spectra of isotopically labeled CCO distinctive. As a consequence of the coupled nature of the ν_1 and ν_2 vibrations of CCO, isotopic substitution at the basal carbon (*CCO) or the oxygen (CC*O) significantly shifts the ν_2 stretch but for the C*CO isotopomer ν_2 is virtually unaffected. Thus, in the ketenylidene complex **1**, ν_2 of the $^{13}C^{12}CO$ isotopomer is 32 cm^{-1} lower in energy than that of the $^{12}C^{12}CO$ species but ν_2 of the $^{13}C^{13}CO$ species is only 6 cm^{-1} lower than that of $^{13}C^{12}CO$. Similarly in the infrared spectrum of matrix-isolated CCO, ν_2 for $^{13}C^{12}C^{16}O$ and $^{12}C^{12}C^{18}O$ is, respectively, 27 and 16 cm^{-1} lower than ν_2 for $^{12}C^{12}C^{16}O$, while ν_2 of $^{12}C^{13}C^{16}O$ is only shifted by 3 cm^{-1} from ν_2 of $^{12}C^{12}C^{16}O$.[25] The origin of these effects is illustrated by the form of the normal modes of CCO derived from the approximate normal-coordinate analysis and displayed in Figure 5. It can be seen that the low-energy CCO stretch (which we refer to in this paper as ν_2) involves primarily motion of the end carbon and oxygen atoms, with very little motion associated with the central carbon atom of the CCO. Hence, the mass of the central carbon atom has only a small effect on the frequency of this particular normal mode.

The implications of the preceding discussion can be transferred to the hypothetical case of CCO on a metal surface. Assuming a CCO disposition more or less perpendicular to the surface, the $^{13}C^{12}C^{16}O$ and $^{12}C^{12}C^{18}O$ isotopomers are predicted to show a significant shift to lower frequency of the ν_2 vibration with respect to ν_2 of $^{12}C^{12}C^{16}O$, while the difference between ν_2 bands of the $^{12}C^{13}C^{16}O$ and $^{12}C^{12}C^{16}O$ isotopomers is predicted to be negligible. In addition, the frequency of the high-energy component ν_1 should be unperturbed by the mass of the basal CCO carbon but significantly affected by changes in the mass of either the central carbon or oxygen atoms.

For CCO formation to occur on a metal, the surface carbide atoms must compete with surface metal atoms for a CO ligand. The C–C bond dissociation energy of ketene is about 80 kcal/mol,[35] and the similarity of the vibrational potential functions of H_2CCO and $[Ru_3(CO)_6(\mu\text{-}CO)_3(\mu_3\text{-}CCO)]^{2-}$ suggests a similar D_{C-C} value for **1**. By comparison, the M–C bond enthalpy for CO bound to a metal surface (measured as ΔH_{ads} for a nondissociated molecule) can be as great as 50 kcal/mol, but ΔH_{ads} for CO on a Ru(100) face ranges between 20 and 30 kcal/mol.[36] By this rough estimate the C–CO bond in the cluster system is stronger than a surface-bound M–CO bond, indicating that CCO formation on a carbided metal surface is thermodynamically feasible. In view of these energy estimates and the many examples of CCO generation by carbide–CO coupling in organometallic clusters, the occurrence of CCO on carbided metal surfaces deserves serious consideration.

Acknowledgment. This research was supported by DOE Grant DE-FG02-86ER13640. M.J.W. was the recipient of a NATO/SERC postdoctoral fellowship.

Supplementary Material Available: Complete listing of the IR bands observed for $[PPN]_2[Ru_3(CO)_6(\mu\text{-}CO)_3(\mu_3\text{-}CCO)]$ from 1600 to 300 cm^{-1} (1 page). Ordering information is given on any current masthead page.

(32) Shincho, E.; Egawa, C.; Naito, S.; Tamaru, K. *Surf. Sci.* **1985**, *155*, 153.
(33) Moon, S. H.; Onuferko, J. H.; Windawi, H.; Katzer, J. R. *J. Vac. Sci. Technol.* **1981**, *18*, 467.
(34) (a) McBreen, P. H.; Erley, W.; Ibach, H. *Surf. Sci.* **1984**, *148*, 292. (b) Mitchell, G. E.; Radloff, P. L.; Greenlief, C. M.; Henderson, M. A.; White, J. M. *Surf. Sci.* **1987**, *183*, 403.
(35) Nuttall, R. L.; Laufer, A. H.; Kilday, M. V. *J. Chem. Thermodyn.* **1971**, *3*, 167.
(36) Somorjai, G. A. *Chemistry In Two Dimensions: Surfaces*; Cornell University Press: Ithaca, NY, 1958; p 290, and references contained therein.